We are IntechOpen, the world's leading publisher of Open Access books Built by scientists, for scientists

4,800
Open access books available

122,000
International authors and editors

135M
Downloads

Our authors are among the

154
Countries delivered to

TOP 1%
most cited scientists

12.2%
Contributors from top 500 universities

WEB OF SCIENCE™

Selection of our books indexed in the Book Citation Index in Web of Science™ Core Collection (BKCI)

Interested in publishing with us?
Contact book.department@intechopen.com

Numbers displayed above are based on latest data collected.
For more information visit www.intechopen.com

Chapter 5

Batteries and Supercapacitors for Electric Vehicles

Monzer Al Sakka, Hamid Gualous, Noshin Omar and Joeri Van Mierlo

Additional information is available at the end of the chapter

http://dx.doi.org/10.5772/53490

1. Introduction

Due to increasing gas prices and environmental concerns, battery propelled electric vehicles (BEVs) and hybrid electric vehicles (HEVs) have recently drawn more attention. In BEV and HEV configurations, the rechargeable energy storage system (RESS) is a key design issue [1–3]. Thus, the system should be able to have good performances in terms of energy density and power capabilities during acceleration and braking phases. However, the thermal stability, charge capabilities, life cycle and cost can be considered also as essential assessment parameters for RESS systems.

Presently batteries are used as energy storage devices in most applications. These batteries should be sized to meet the energy and power requirements of the vehicle. Furthermore, the battery should have good life cycle performances. However, in many BEV applications the required power is the key factor for battery sizing, resulting in an over-dimensioned battery pack [4,5] and less optimal use of energy [4]. These shortcomings could be solved by combination of battery system with supercapacitors [6–8]. In [9], it is documented that such hybridization topologies can result into enhancing the battery performances by increasing its life cycle, rated capacity, reducing the energy losses and limiting the temperature rising inside the battery. Omar et al. concluded that these beneficial properties are due to the averaging of the power provided by the battery system [4,6,9]. However, the implementation of supercapacitors requires a bidirectional DC–DC converter, which is still expensive. Furthermore, such topologies need a well-defined energy flow controller (EFC). Price, volume and low rated voltage (2.5–3 V) hamper the combination of battery with supercapacitors [6,10]. In order to overcome these difficulties, Cooper et al. introduced the Ultra-Battery, which is a combination of lead-acid and supercapacitor in the same cell [11]. The new system encompasses a part asymmetric and part conventional negative plate. The proposed system allows

to deliver and to absorb energy at very high current rates. The Ultra-Batteries have been tested successfully in the Honda Insight. However, this technology is still under development. In the last decade, a number of new lithium-ion battery chemistries have been proposed for vehicular applications. In [12–15], it is reported that the most relevant lithium-ion chemistries in vehicle applications are limited to lithium iron phosphate (LFP), lithium nickel manganese cobalt oxide (NMC), lithium nickel cobalt aluminum oxide (NCA), lithium manganese spinel in the positive electrode and lithium titanate oxide (LTO) in the negative electrode. In this chapter, the performance and characteristics of various lithium-ion based batteries and supercapacitor will be evaluated and discussed. The evaluation will be mainly based on the electrical behavior. Then the characteristics of these RESS systems will be investigated based on the electrical and thermal models.

2. Batteries

2.1. Electrical characterization

It is well known that the key consideration in the design of rechargeable energy storage systems in PHEV and BEV applications mainly depend on the power density (kW/kg) and energy density (Wh/kg) due to the design concept. However, the battery technology also should be able to have good performances in the terms of energy efficiency, lifetime, and charging rate [12-15]. In this section all these parameters have been analyzed for 10 lithium-ion battery types as presented in Table 1.

	A	B	C	D	E	F	G	H	I	J
Cathode	LFP	LFP	LFP	NMC	NMC	NCA	LFP	LFP	LFP	LFP
Shape	Cylindrical	Pouch	Pouch	Pouch	Pouch	Cylindrical	Pouch	Cylindrical	Prismatic	Prismatic
Nominal capacity [Ah]	10	10	40	12	70	27	14	2.3	10	40
Nominal voltage [V]	3.3	3.3	3.3	3.7	3.7	3.7	3.3	3.3	3.3	3.3

Table 1. Specifications investigated lithium-ion battery brands [12].

In [16] the main design concepts of PHEV applications are discussed, compared to the three sets of influential technical goals, and explained the trade-offs in PHEV battery design. They mentioned that the energy and power requirements according to the U.S. Advanced Battery Consortium (USABC) should be in the range of 82 Wh/kg and 830 W/kg for PHEV-10 and 140 Wh/kg and 320 W/kg for PHEV-40. Pesaran specified these two battery types as high power/energy ratio battery (PHEV-10) and low power/energy battery (PHEV-40). The first category PHEV-10 is set for a "crossover utility vehicle" weighing 1950 kg and PHEV-40 is set for a midsize sedan weighing 1600kg [16]. In this study, only the battery performance

http://dx.doi.org/10.5772/53490

characteristics for PHEV-40 (40 miles All Electric Range) is investigated based on the USABC goals [16].

Figure 1 shows the results of the Dynamic Discharge Performance test (DDP) and the Extended Hybrid Pulse Power Characterization (HPPC) test [12,17-19]. As one can see, the energy density of nickel manganese cobalt oxide (LiNiCoMnO2) based battery types D&E is in the range of 126 – 149Wh/kg while the cells using iron phosphate in the positive electrode show energy density being in the range of 75 – 118Wh/kg. In [20], is reported that the high energy density values for the $LiNiCoMnO_2$ batteries is mainly due to the higher nominal voltage (e.g. 3.7V) and good electrode specific capacities. However, the situation regarding the power density is not clear due the fact that power is varying over a wide range. Figure 1 shows that only cell type D using $LiNiCoMnO_2$ has the highest power density around 2100Wh/kg. This result is mainly due to the good specific impedance [20].

The results indicate also that iron phosphate based battery types B and H have good power performances being in the range of 1580-1650 W/kg. However, based on the USABC goals, all the tested cells can meet the power requirements of 320W/kg with exception of battery F 290W/kg. Although the battery type E has the best energy density, the power capabilities of this battery are limited in comparison to the batteries types B, D and H, which indicates that this battery is more appropriate for BEV applications as reported in [12]. The presented results in Figure 1 are based on the maximum discharge C-rate at 50% state of charge.

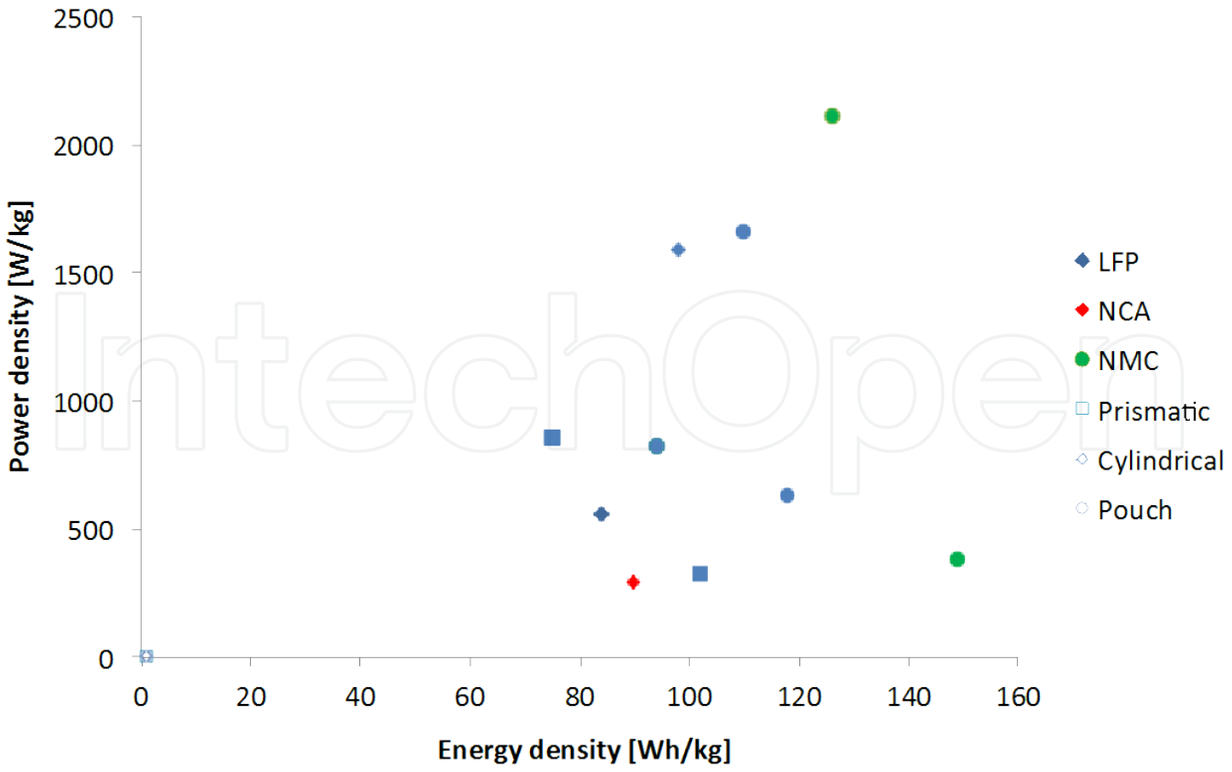

Figure 1. Power density versus energy density at room temperature [12].

2.1.1. Energy efficiency

In PHEV applications, energy efficiency during charge and discharge phases can be considered as one of the key factors. High-energy efficiency is desired to limit the temperature rise inside a battery pack. In this section, the energy efficiency of the proposed battery types has been considered based on the DDP test [19].

It is well pointed out in Figure 2, that the energy efficiency of the nickel manganese cobalt oxide based cells is around 94 – 96%. While the iron phosphate and nickel cobalt aluminum in the positive electrode show generally a lower efficiency in the range of 88 – 93%. The lower energy efficiency for lithium iron phosphate based batteries can be explained due to the relative lower conductivity of cathode material compared to NMC based batteries.

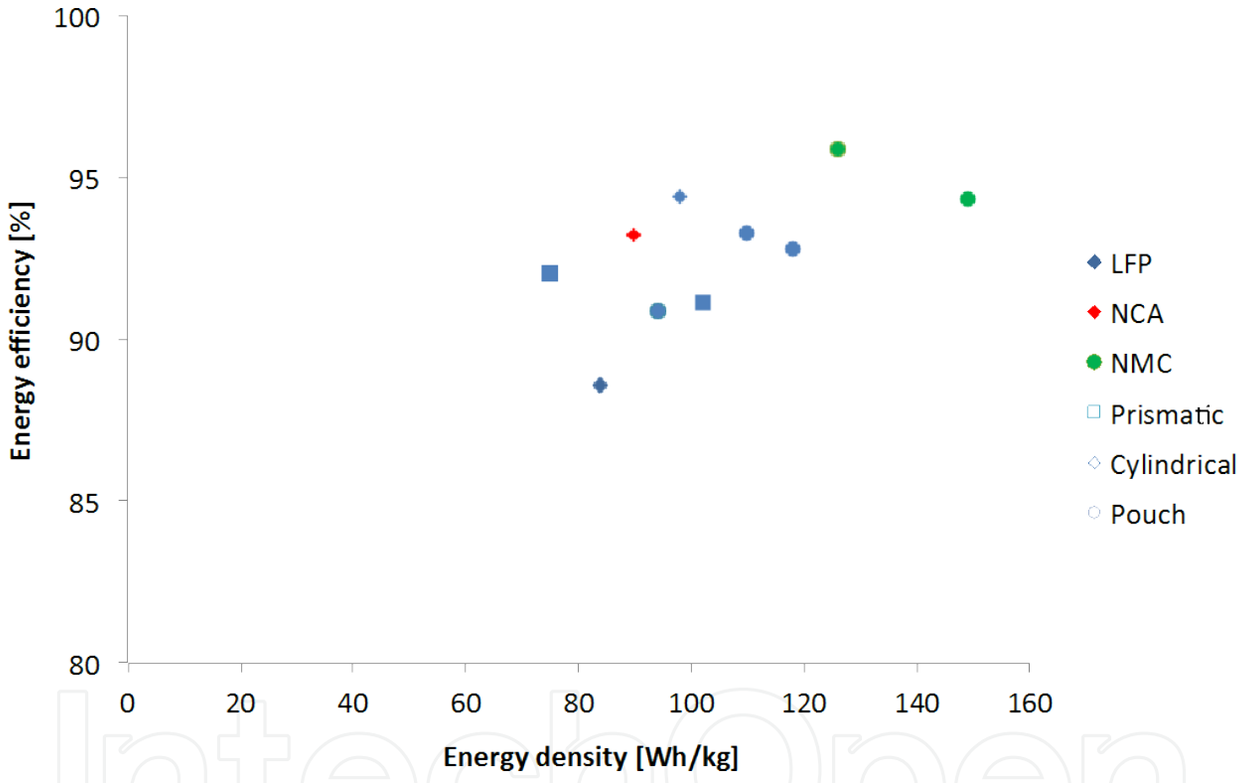

Figure 2. Energy efficiency versus energy density at room temperature [12].

2.1.2. Charge performances

It is generally known that PHEV applications are an important factor for improving the impact of traffic on healthier living environment by emitting a lower amount of CO_2 than the conventional vehicles. However, the advantages of PHEV applications mainly depend of the energy storage device. On the other hand, in order to enhance the suitability of the battery technology in PHEV applications, the battery requires besides good power, energy and energy efficiency performances also acceptable fast charging capabilities. In [21], it is well reported that the charging process of battery typically involves two phases:

http://dx.doi.org/10.5772/53490

- The main charging phase, where the bulk of energy is recharged into the battery (constant current),
- The final charge phase, where the battery is conditioned and balanced (constant voltage).

In this section, the fast charging performances of the different batteries until the main charging phase have been analyzed. In this study the main charging phase has been considered at different charge current rates (0.33 I_t, 1 I_t, 2 I_t and 5 I_t). The reference test current I_t can be expressed as according to the standard IEC 61434 [22]:

$$I_t[A] = \frac{C_n[Ah]}{1h} \quad (1)$$

Figure 3 shows clearly that lithium-ion battery technology have high charge performances. For most lithium-ion batteries, the stored capacity up to V_{max} is above 60% at 5 I_t. Due to the higher charge current rates, the charge time can be reduced with a factor 10. The discharge time is less than 1 hour instead of 8 hours as mentioned in [15]. Here it should be noted that battery cells with high energy density, which are designed for BEVs and PHEVs show high performances between 1 I_t and 2 I_t but indicate less performances at higher current rates (> 2 I_t) [12].

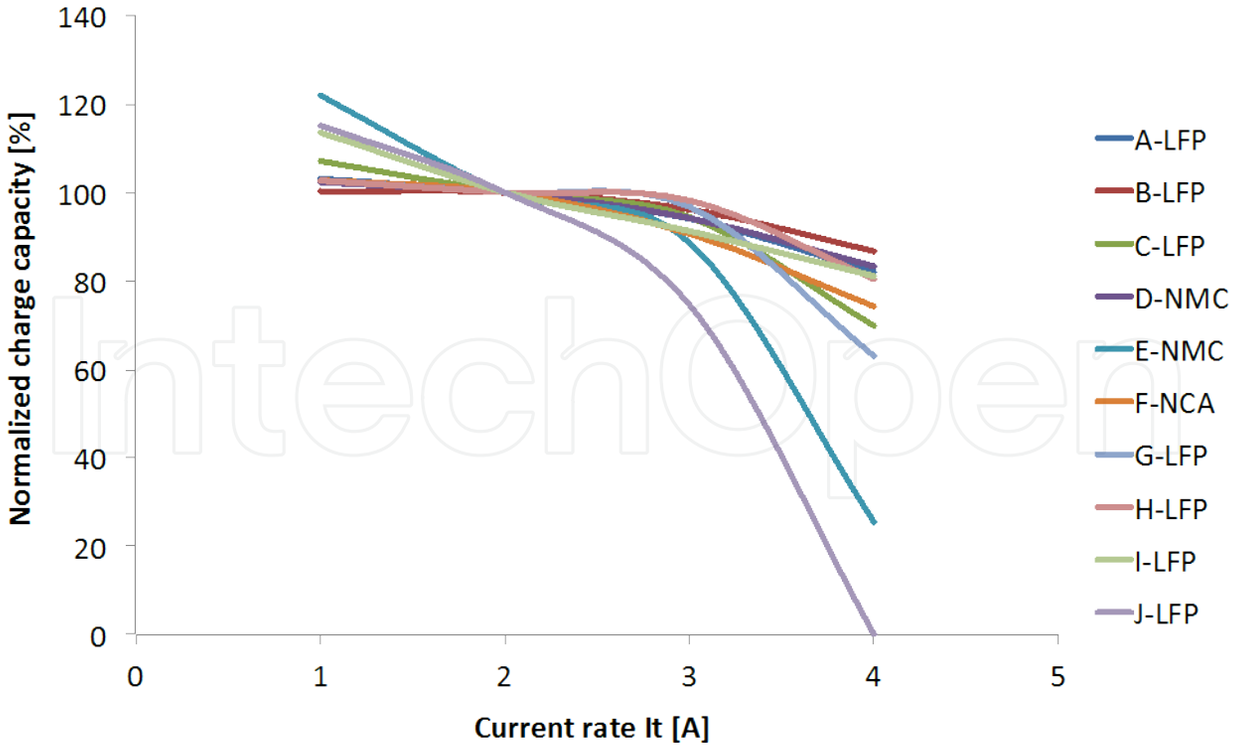

Figure 3. Evolution of stored capacity during main charging phase [12].

2.2. Thermal characterization

According to the United States Advanced Battery Consortium, the battery system in HEVs, PHEVs and BEVs should operate over a wide operating temperate (from -40°C until 60°C) In order to illustrate the battery behavior at different working temperatures, the same dynamic discharge performance test as described above has been performed at -18°C, 0°C, 25°C and 40°C as described in the standard ISO 12405-1/2 and IEC 62660-1 [23-25].

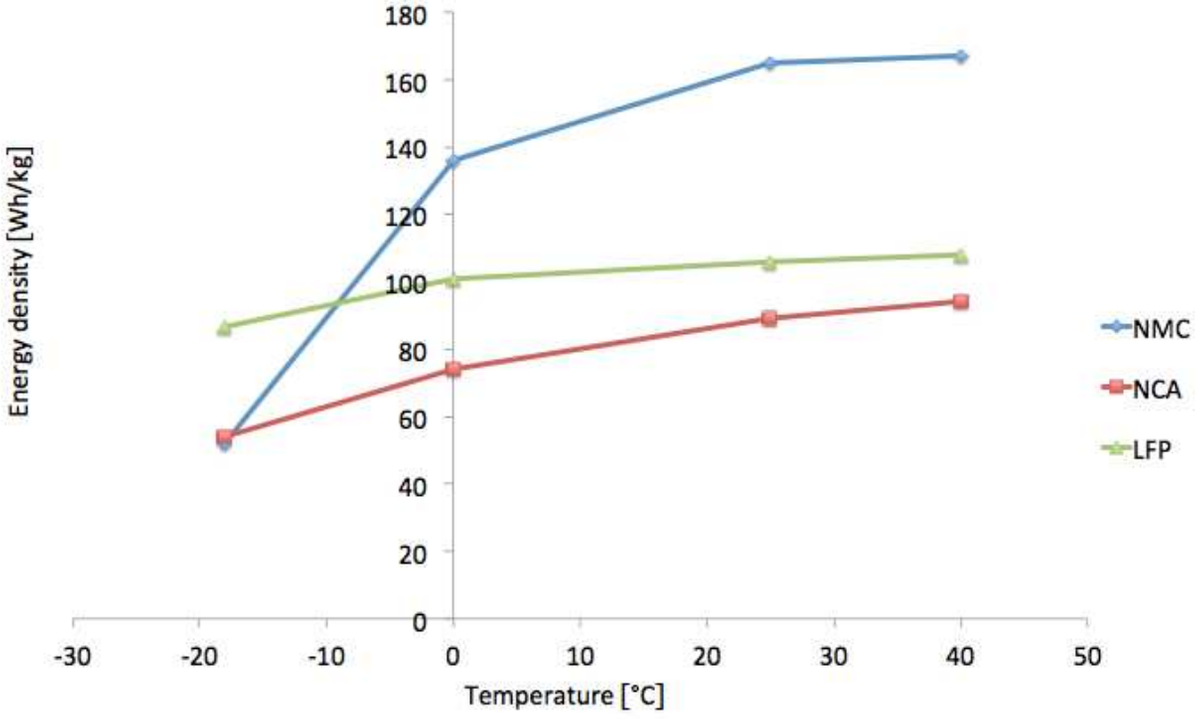

Figure 4. Evolution of energy density as function of working temperature [14].

Figure 4 illustrates that the nickel manganese cobalt oxide based battery (type E) has an energy density of 150-125 Wh/kg in the temperature range of 40°C and 0°C. While the energy density of lithium iron phosphate (type H) and lithium nickel cobalt aluminum oxide in the positive electrode (type F) seem to have less favorable performances 108-101 Wh/kg for LFP and 94 74 Wh/kg, for NCA. However, the performances at -18°C are less beneficial for NMC battery type around 50 Wh/kg against 54 Wh/kg and 86 Wh/kg for NCA and LFP, respectively. These results show that the energy density reduction is 60% for NMC, 40% for NCA and 20% for LFP cells. This means that a heating system will be more than desired for NMC and NCA cells in order to keep the battery cells in the appropriate temperature envelope (40°C-0°C), where the energy performances are relative high. The high energy density in the case of NMC at 40°C and 25°C are due to the good specific capacity and the higher nominal voltage. The obtained energy density for nickel cobalt aluminum in the positive electrode is quite small against what is documented by Burke [9]. The reason is that the investigated cells (see Table 1) are dimensioned for hybrid applications rather than battery propelled

http://dx.doi.org/10.5772/53490

electric vehicles. In [26] is reported that the limitation of the energy density at low temperatures is mostly related to the considerable increasing of the internal resistance. However, Figure 5 indicates that the aspect does not apply for LFP based battery. The normalized internal resistance increases in the case of the latter mentioned cell chemistry is 650% compared at the reference temperature (25°C). The internal resistance has been determined at 100% SoC and the applied current was 0.1 I_t and 1 I_t.

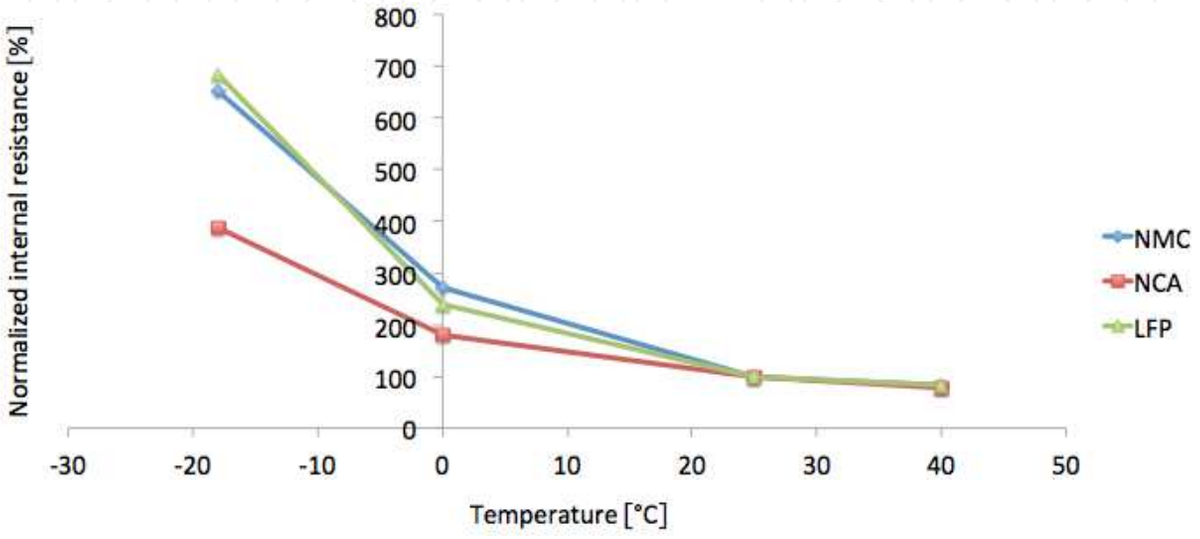

Figure 5. Evolution of the internal resistance as function of the working temperature [14].

In order investigate the behavior of the proposed LFP and NMC based batteries in depth, a number of capacity tests have been carried out at current rates 2 I_t, 5 I_t and 10 I_t at 0°C. Figure 6 and Figure 7 show the favorable performances of the LFP chemistry against the NMC. Especially at 0°C, the LFP battery demonstrates the excellent performances due to the self-heating mechanism that occur at high current rates. In Figure 6, we observe that the voltage at 10 I_t drops fast but remains above the minimal voltage: 2V. Then, the voltage recovers when the battery temperature considerable increases (43°C) due to the higher internal resistance. The battery is able to attain almost the same discharge capacity as at lower current rate and high working temperature as it is illustrated in Figure 8. Here, we can notice that the Peukert number in the temperature range (0°C – 40°C) is close to one as is reported by Omar et al. [7]. However, at low temperatures (-18°C and forward) the Peukert number increases (1.85) due to the reducing of the discharge capacity, which is caused by the significantly high internal resistance. It should be pointed out that in the region 0.33 I_t and 2 I_t, the Peukert number is smaller than 1, which is in contradiction with the Peukert phenomena. The explanation of this behavior is due to the fact that the Peukert relationship has been extracted particularly for lead acid batteries and for relative low current rates and in operating temperatures, which is close to the room temperature. However, for lithium-ion batteries and mainly at low temperatures (-18°C), there are another complex phenomena that occur that only cannot be explained by Peukert.

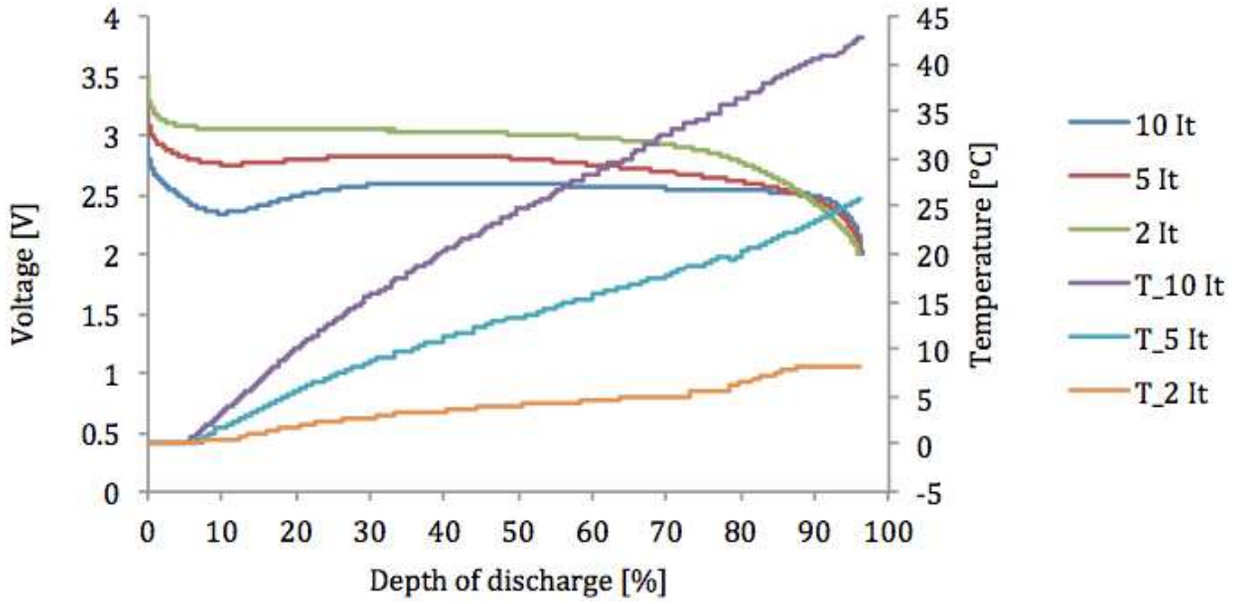

Figure 6. Illustration of the voltage and temperature evolution of LFP based battery versus depth of discharge at different current rates at 0°C [14].

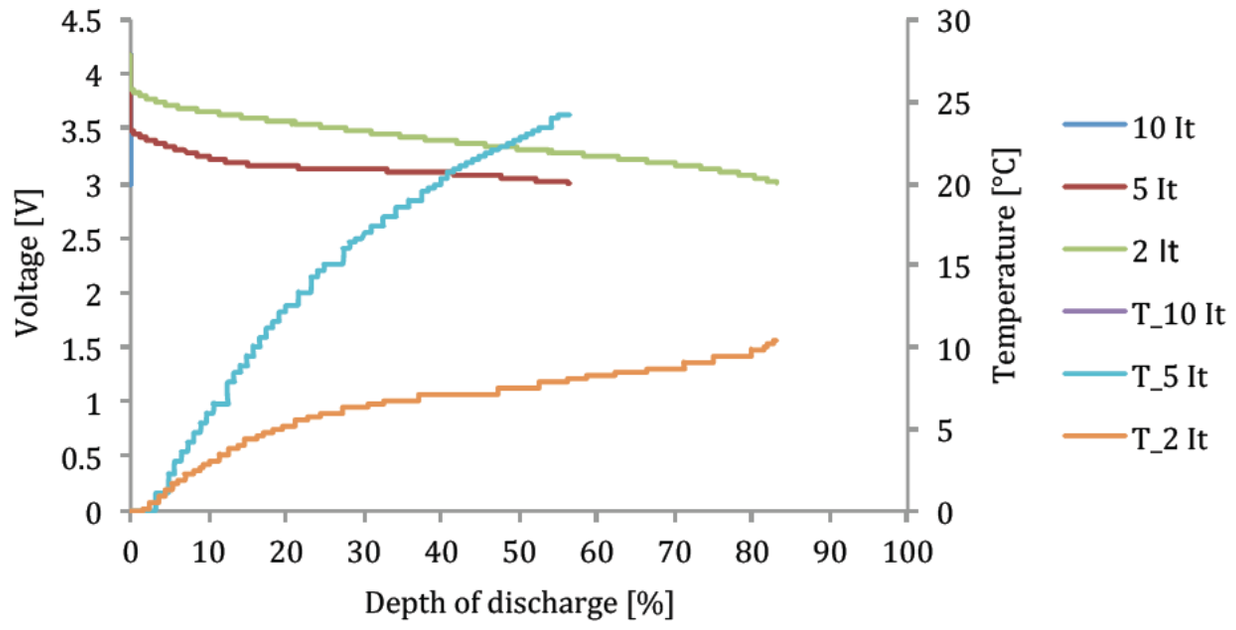

Figure 7. Illustration of the voltage and temperature evolution of NMC based battery versus depth of discharge at different current rates at 0°C [14].

2.3. Electrical and thermal modeling

In development of an appropriate battery pack system, the battery management system can be assumed as a key system [27]. The accuracy and the performances of this system depend on the developed balancing system and an accurate electrical and thermal battery model

http://dx.doi.org/10.5772/53490

which can predict the battery cell behavior under all operational conditions. The electrical model is required for prediction of the battery behavior such as energy, power, internal resistance, life cycle and energy efficiency. On the other hand the thermal model is needed to predict the surface temperature of the battery cell for operating of the cooling and heating system when required. Further, the output of the thermal model will be used as an input for the electrical model due to the dependency of the model parameters as a function of the temperature. In this section the performances of the well-known first order FreedomCar battery model will be analyzed by using a dedicated test protocol and a new estimation technique. Then, the analysis is extended with a novel developed thermal model that has been developed at the Vrije Univeriteit Brussel for lithium-ion batteries.

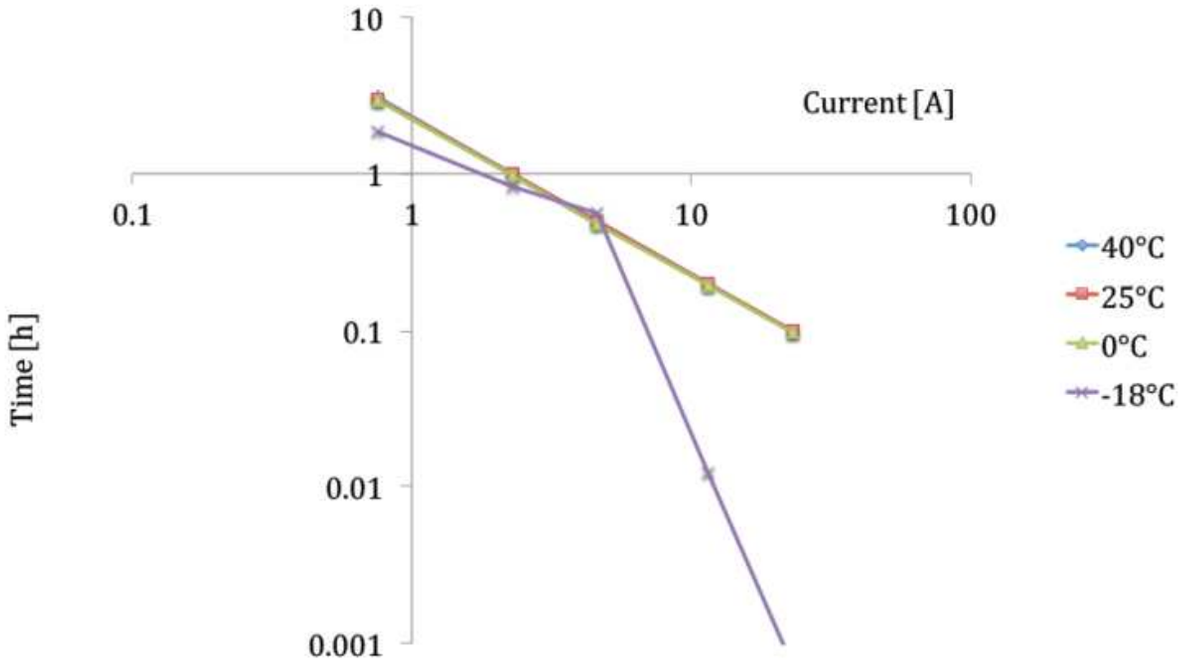

Figure 8. Illustration of the Peukert as function of the operating temperature (LFP) [14].

2.3.1. Electrical model: FreedomCar battery model

As reported above, the BMS requires an accurate electrical battery model for prediction of the battery behavior during the short and long term. Therefore, in the literature, one can find a number of electrical models such as Thévenin, FreedomCar, second order FreedomCar and RC battery model [28, 29]. The Thévenin battery model is a modified model of the FreedomCar battery model as it is presented in Figure 9. The Thévenin model is during steady state operations less accurate than the FreedomCar model due to the absent of the fictive capacitor 1/OCV'. The second order FreedomCar battery model has relatively higher performances than the Thévenin battery model, but this model is also more complicated due to the present of two RC-circuits in the system, which seems in the reality too heavy for BMS in PHEVs and BEVs where 100 battery cells are connected in series. Therefore, the processing unit should be very powerful.

In the framework of this section, only the characteristics of the first order FreedomCar battery model will be addressed and compared with experimental results. As it presented in Figure 9, the FreedomCar model exists mainly of an ohmic resistance (R_o), a fictive capacitor (1/OCV') which represents the variation of the voltage over the time, an open circuit voltage OCV and a RC circuit existing of a polarization resistance R_p and capacitor C. The model assumes that the battery model parameters should be as function of state of charge and temperature. However, the researchers at the Vrije Universiteit Brussel found that the impact of the current rate and cycle life are also important parameters that cannot be avoided [28]. Then, the researchers found also that the ohmic resistance should be divided into two parts: the charge ohmic resistance and the discharge ohmic resistance due to the battery hysteresis [28].

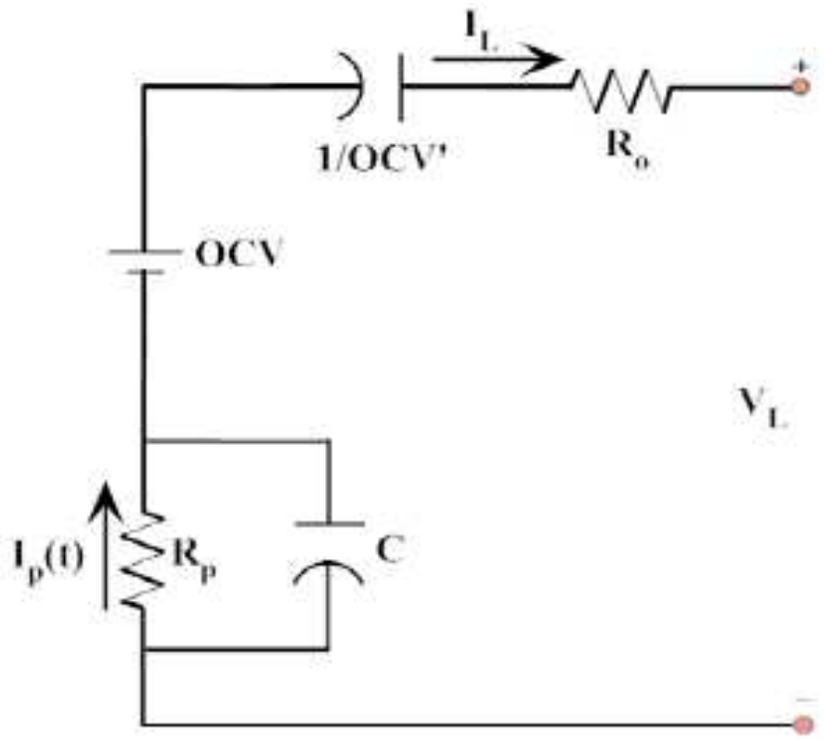

Figure 9. First order FreedomCar battery model [28].

2.3.2. Calibration and validation results

Prior starting with validation of the proposed battery model, the model has been calibrated by performing a new developed test profile at the Vrije Universitiet Brussel as it is presented in Figure 10. As we can observe, there is a good agreement between the simulation and the experimental results. According to these results, the error percentage is not higher than 3.5%. This indicates the powerful performances of the proposed battery model with the developed estimation technique.

http://dx.doi.org/10.5772/53490

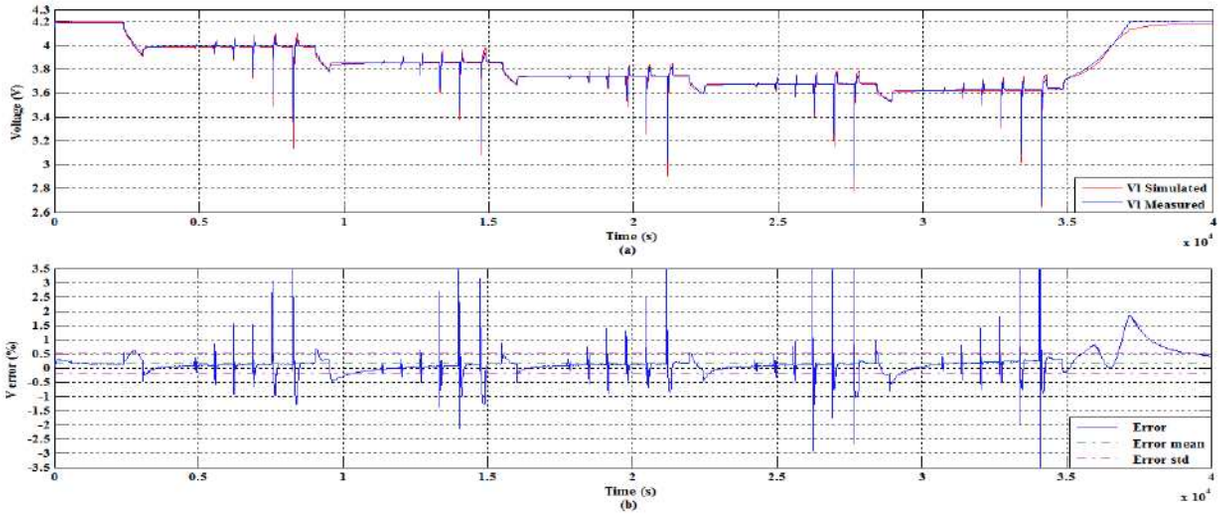

Figure 10. Calibration of the first order FreedomCar battery model at room temperature [28].

2.3.3. Thermal model

Regarding the prediction the thermal behavior of a battery, this can be performed by using high accurate thermal sensors or by dedicated thermal battery models. However, thermal models have many advantages against thermal sensors. The sensors can only measure one specific point. As it is generally know the heat distribution over the surface temperature of the battery is not uniform. In order to have a good sight of the heat development inside the battery, several thermal sensors are needed. This issue will complicate the BMS and the processing time of the BMS will be significantly longer. Therefore, it is more of high interest to issue thermal model which can predict the heat development and distribution over the battery surface. Further, such models allow in advance the battery pack designer to investigate the weakness in the battery pack and to dimension the cooling system more accurately. Finally, the development cost of such battery model is less than the cost of the significant higher number thermal sensors that are needed. In this perspective, a novel thermal model has been developed at the Vrije Universiteit Brussel that can be used for lithium-ion batteries and supercapacitors [30, 31]. In Figure 11 the thermal model is illustrated. As we can observe, the model exists of the following components [30, 31]:

- P_{gen} represents the heat generation (irreversible heat)
- C_{th} stands for the thermal capacitance,
- R_{thi} is the thermal resistance,
- R_{con} represents the convection thermal resistance,

2.3.4. Calibration and validation results

In order to verify the developed thermal battery model, series of comparisons are made based on simulation and experimental results. The first test is presented in Figure 12. As we

observe, the model is in good agreement with experimental results. The errors percentage based on this test is in the range of 1°C. In this test, the model has been compared with experimental results based on the load profile as proposed in Figure 13 until the surface temperature has reached the steady stated condition.

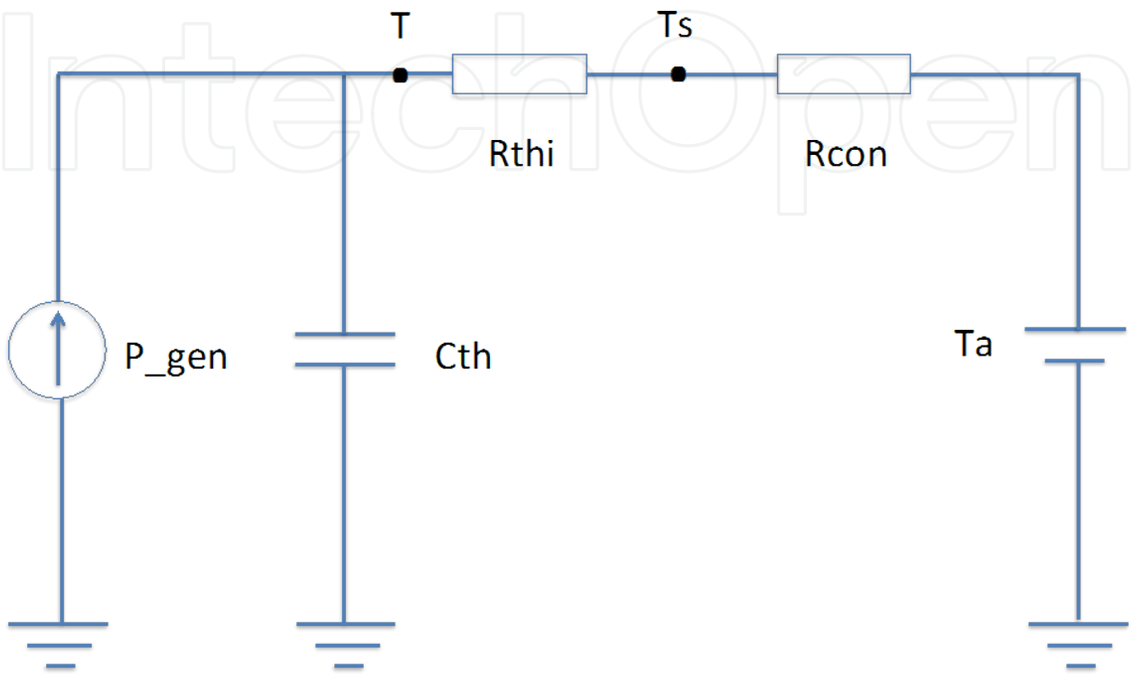

Figure 11. Novel thermal batter model for lithium-ion batteries and electrical double-layer capacitors [30].

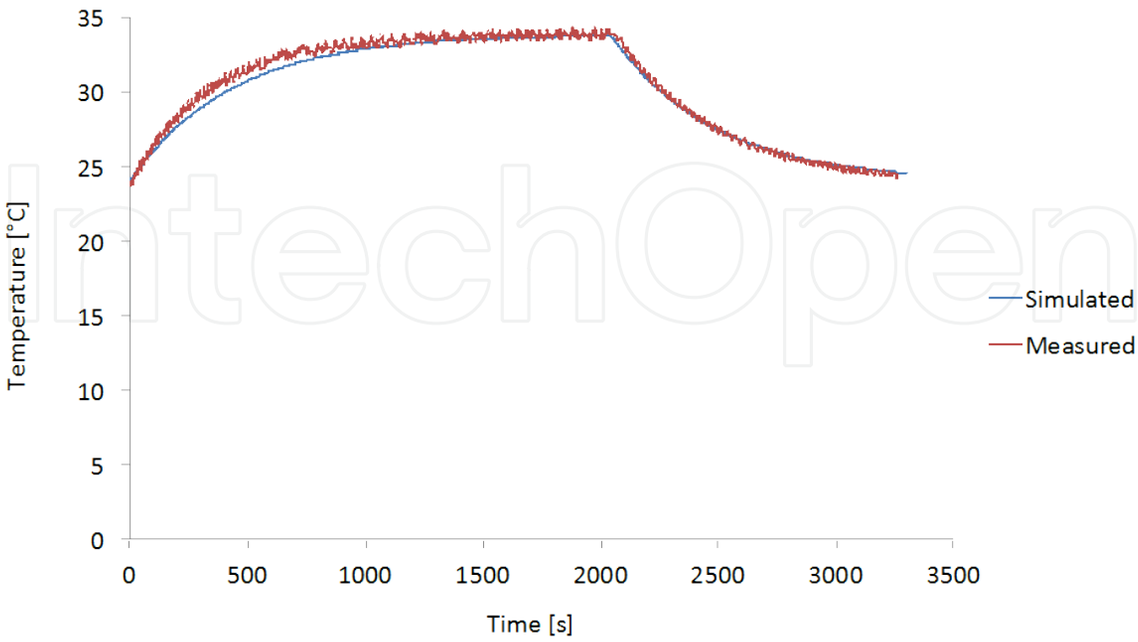

Figure 12. Comparison of simulated and measured at 25°C working temperature [30].

http://dx.doi.org/10.5772/53490

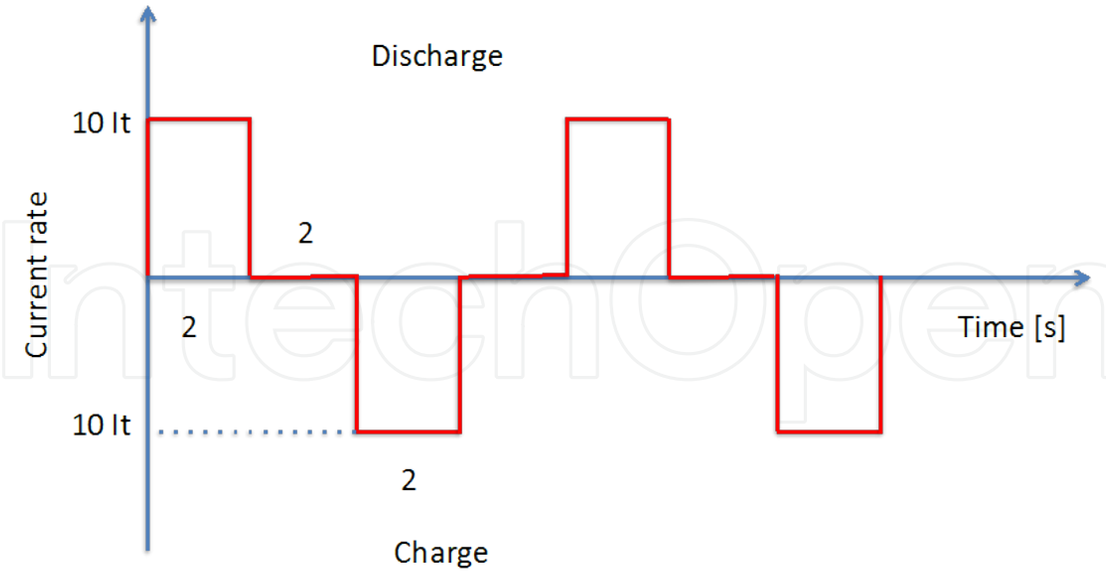

Figure 13. Used load profile for extraction of the thermal model parameters [30].

However, there is a need for validation step to evaluate the performances and accuracy of the developed battery model at other conditions without to perform any calibration in the model. In Figure 14 a validation test has been carried out at room temperature about 24°C. The corresponding simulation and experimental comparison are illustrated in Figure 15. Here again, we recognize that the high accuracy of the battery model against the experimental results. Based on these results, we can conclude that the developed battery model is able to predict the surface temperature of the battery cell with significantly low errors.

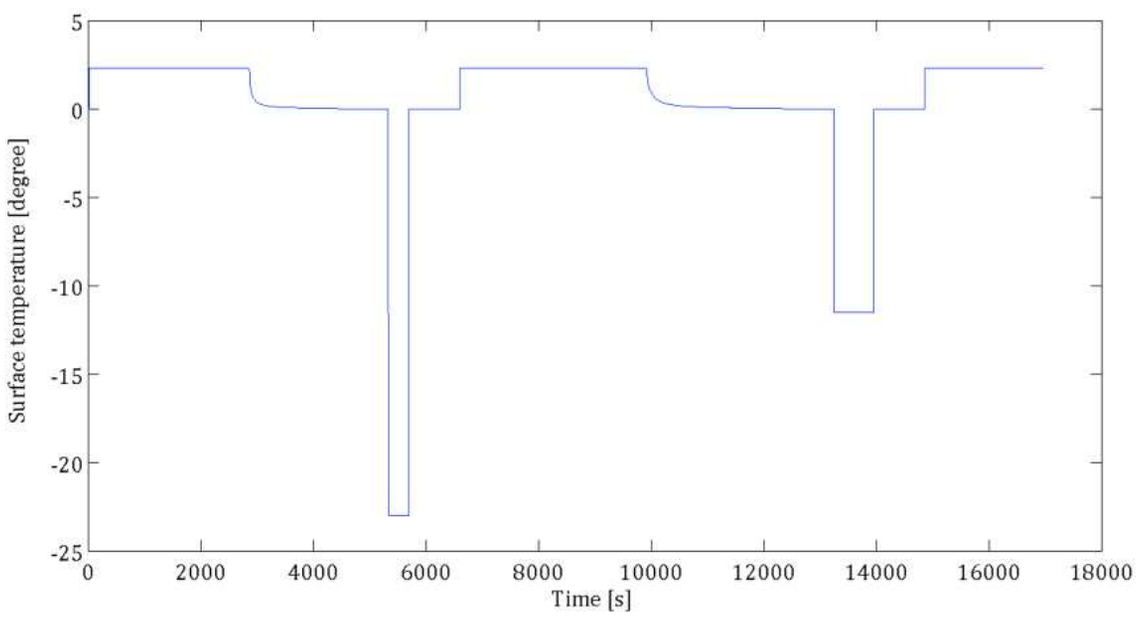

Figure 14. Load profile for validation [30].

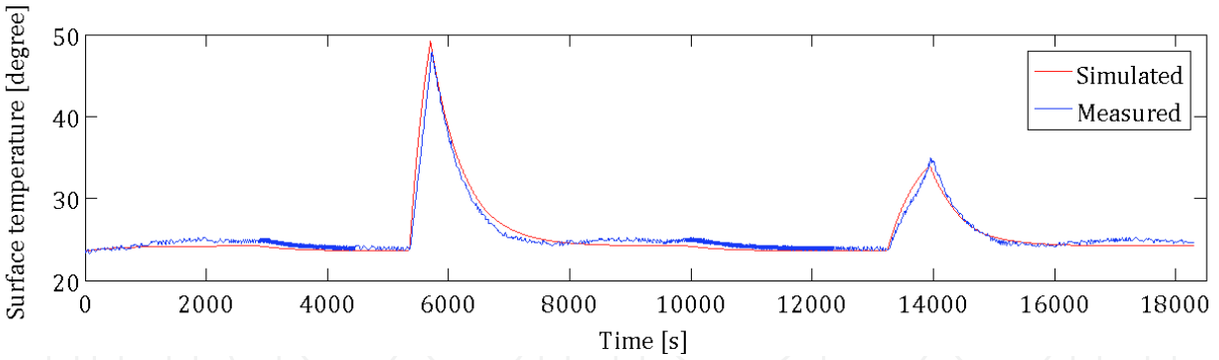

Figure 15. Comparison of experimental and simulation results at room temperature (~24°C) [30].

3. Supercapacitors

Supercapacitors, also known as Electric Double-Layer Capacitors (EDLCs)or ultra capacitors, have a high energy density when compared to conventional capacitors, typically thousands of times greater than a high capacitance electrolytic capacitor. For example, a typical electrolytic capacitor will have a capacitance in the range of tens of milli-farads. The same size supercapacitor would have a capacitance of several farads. Larger supercapacitors have capacitance up to 5000 farads. The highest energy density in production is 30 Wh/kg. Although supercapacitors have very high power density and capacitance values of thousands of Farads are possible, the cell voltage is limited to about 2.7 V to avoid electrolysis of the electrolyte with the consequent emission of gas and deterioration of the supercapacitor cell. The structure of a basic cell is mostly cylindrical. However, there are also now commercial pouch supercapacitors available. The technology achievement is identical to that used for conventional capacitors. The supercapacitors cells used in this study are the BCAP310F and BCAP1500F. Their properties are based on the double layer capacitance at the interface between a solid conductor and an electrolyte. The elementary structure consists of two activated carbon electrodes and a separator impregnated with an electrolyte. The electrodes are made up of a metallic collector, coated on both side with an active material, which has a high surface area part which is required for the double layer. The two electrodes are separated by a membrane (separator), which prevents the electronic conduction by physical contact between the electrodes but allows the ionic conduction between them. This composite is subsequently rolled and placed into a cylindrical container. The system is impregnated with an organic electrolyte. The two electrodes are metalized and connected to the outside (+) and (-) terminal connections of the supercapacitor.

3.1. Electrical characterization

Equivalent series resistance and capacitance of supercapacitor calculation methods:

http://dx.doi.org/10.5772/53490

3.1.1. Using an Electrochemical Impedance Spectroscopy (EIS)

Electrochemical impedance spectroscopy (EIS) is used in the characterization of electrochemical behavior of energy storage devices. Impedance analysis of linear circuits is much easier than analysis of non-linear ones. Electrochemical cells are not linear. Doubling the voltage will not necessarily double the current. However, the electrochemical systems can be pseudo-linear. In normal EIS practice, a small (1 to 10 mV) AC signal is applied to the cell. With such a small potential signal, the system is pseudo-linear.

The supercapacitor is polarized with a dc voltage. A small voltage ripple, typically 10mV, is superimposed on the dc component. The ripple frequency is swept between 1 mHz and 1 kHz. The measurement of the current amplitude and phase with respect to the injected voltage permits the determination of the real and imaginary components of the impedance as a function of the frequency. The measurements were performed in a controlled climatic chamber. The supercapacitor capacitance C and the series resistance (ESR) are deduced from the experimental results, respectively.

$$C = \frac{-1}{2\pi \cdot \mathrm{Im}(z) \cdot f} \tag{2}$$

$$ESR = \mathrm{Re}(z) \tag{3}$$

Where:

- Im(z) is the imaginary component of the supercapacitor impedance,
- Re(z) is the real component of the supercapacitor impedance,
- F is the frequency.

The Maxwell BCAP310F and BCAP1500F supercapacitors used in this study are based on activated carbon technology and organic electrolyte. These devices were characterized using the Electrochemical Impedance Spectroscopy (EIS) [32].

Figure 16 and Figure 17 represent the BCAP310F and the BCAP1500F capacitance and ESR as a function of frequency.

At low frequency, the capacitance is maximum, for example at 10mHz the capacitance value is in order of 1660F for the BCAP1500F and 315F for the BCAP310F. At 50mHz the ESR value is in order of 1mΩ for BCAP1500F and 5.2mΩ for BCAP310F. The BCAP310F ESR is relatively high because this device was fabricated, by Maxwell Technologies, especially for these thermal tests; it is including 4 thermocouples type K inside.

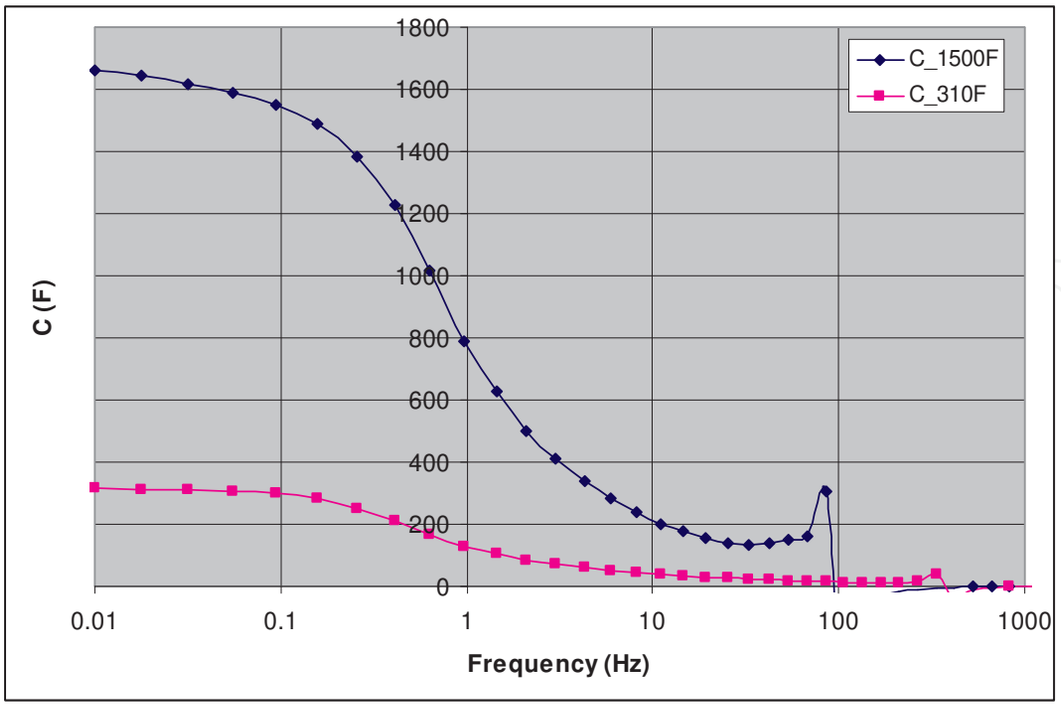

Figure 16. BCAP1500F and BCAP310F capacitance as function of frequency with a bias voltage respectively of 2.7V and 2.5V and a temperature of 20°C.

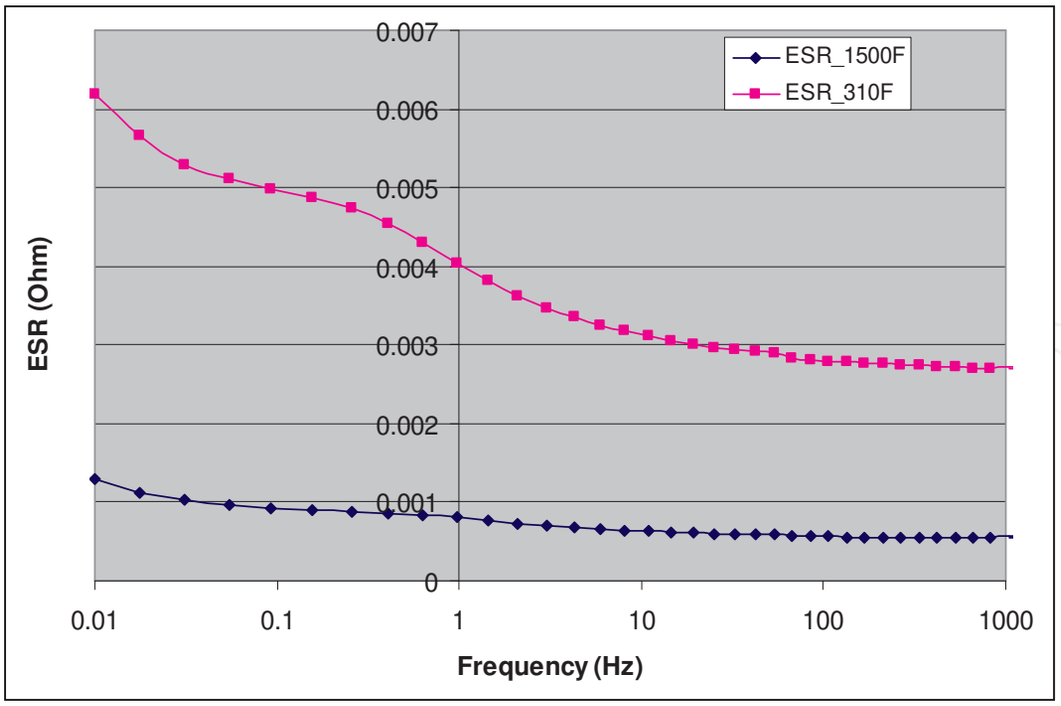

Figure 17. BCAP1500F and BCAP310F series resistance as function of frequency with a bias voltage respectively of 2.7V and 2.5V and a temperature of 20°C.

http://dx.doi.org/10.5772/53490

3.1.2. Based on the IEC 62576 standard

The standard IEC (International Electro-technical Commission) 62576 [33,34] defines the calculation methods of the equivalent series resistance and the capacitance of electric double-layers capacitors.

Figure 18 presents the calculation method of the equivalent series resistance. The supercapacitor is charged at constant current to its nominal voltage, this voltage should be maintained at this value during 30 min. Then, the supercapacitor is discharged at constant current up to 0V. The value of the constant current depends on the applications. The IEC 62576 suggests to choose 10xC, 4xCxUr, 40*C*Ur and 400xCxUr mA for the supercapacitors applied as memory backup (class 1), energy storage (class 2), power unit (class 3) and instantaneous power unit (class 4), respectively [33,34]. Where, C is the capacitance and Ur represents the rated voltage.

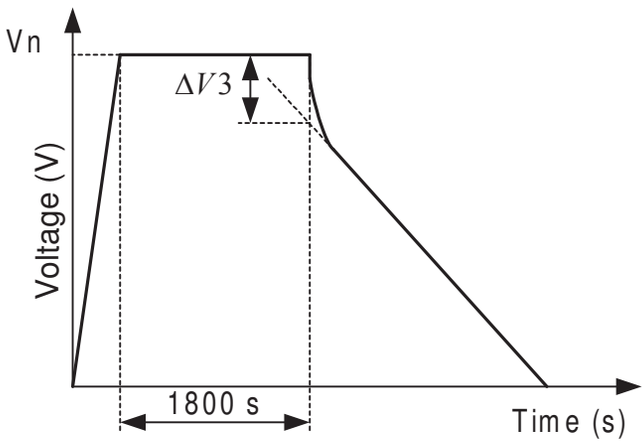

Figure 18. Charge and discharge of the supercapacitor at constant current

The ESR value is calculated based on the following expression:

$$ESR = \frac{\Delta V3}{I} \tag{4}$$

Where ΔV3 is the voltage drop obtained from the intersection of the auxiliary line extended from the straight part and the time base when the discharge starts, and I is the constant discharging current.

Figure 19 presents the calculation method of the capacitance.

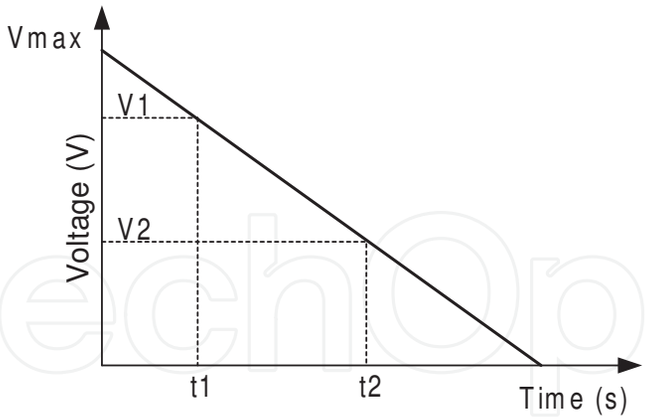

Figure 19. Discharge at constant current of the supercapacitor

The capacitance value is calculated using the following expression:

$$C = \frac{I \cdot \Delta t}{\Delta V} \tag{5}$$

Where I is the constant discharging current, Δt=t2-t1 and ΔV=V1–V2, V1=80%*Vmax, V2=40%*Vmax and Vmax is the maximum voltage of the supercapacitor.

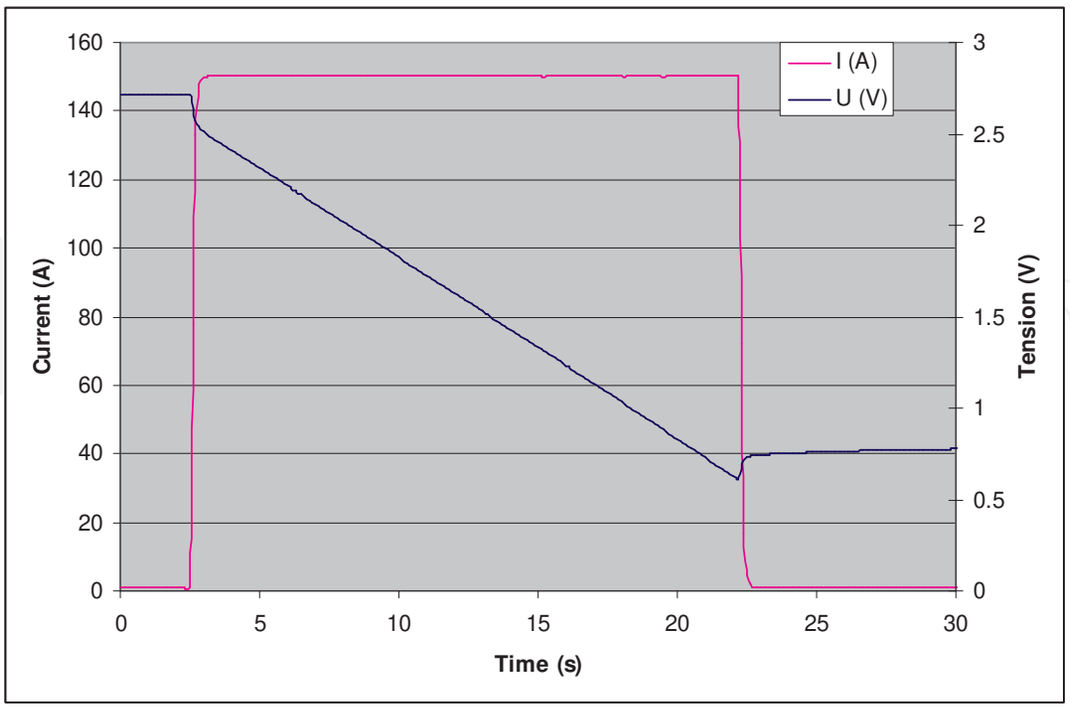

Figure 20. Experimental results of BCAP1500F voltage and current as a function of time.

http://dx.doi.org/10.5772/53490

The BCAP1500F capacitance and ESR were calculated according to the IEC 62576 standard. The supercapacitor is discharged at constant current 100mA/F. Figure 20 represents the BCAP1500F voltage and current versus time during the discharge. ESR and C are 1.07mΩ and 1525F, respectively.

3.2. Thermal characterization

Heat production in supercapacitor is related exclusively to Joule losses. The supercapacitors support currents up to 400A or more depending on cell capacitance and used technology. The repetitive charge and discharge cycles of the supercapacitor cause a significant warming even though the equivalent series resistance value is around the mΩ according to the capacitance. Several authors showed that the supercapacitor ESR varies according to the temperature [35-37]. In [38] the authors have studied the effect of the temperature and the voltage on the supercapacitors ageing. They have established a model which allows analyzing self-accelerating degradation effects caused by elevated voltages and temperatures, this model is a holistic simulation model that combines electrical and thermal simulation of supercapacitor modules with an ageing model.

In the reference [39] the authors have studied and modeled the temperature effect on the supercapacitor self discharge.

This rise in temperature can have the following consequences:

- The deterioration of the supercapacitor characteristics, especially ESR, self discharge and lifetime [39,40], which affect its reliability and its electrical performance.
- The pressure inside the supercapacitor is increased.
- A premature aging of metal contacts, in fact the repetitive heating and significant temperatures can deteriorate rapidly the terminal connections of the supercapacitor.
- The evaporation of the electrolyte and hence the destruction of the supercapacitor if the temperature exceeds 81.6°C which is the boiling point of the electrolyte.

Therefore, it is important to know and understand the heat behavior of supercapacitor cells and modules. This leads to an estimation of the space-time evolution of the temperature.

This study deals with the thermal modeling and heat management of supercapacitor modules for vehicular applications. The thermal model developed is based on thermal-electric analogy and allows the determination of supercapacitor temperature. Relying on this model, heat management in supercapacitor modules was studied for vehicle applications. Thus, the modules were submitted to real life driving cycles and the evolution of temperatures of supercapacitors was estimated according to electrical demands. The simulation results show that the hotspot is located in the middle of supercapacitors module and that a forced airflow cooling system is necessary.

For supercapacitor thermal behavior, the device was characterized by using the EIS for different temperature. Figure 21 presents the Maxwell BCAP0310F ESR variations according to the temperature. The ESR increases at negative temperature values. The ESR variation is higher for negative temperature than for positive one. This is due to the fact that the electro-

lyte's conductivity is strongly temperature dependent. Above 0°C ESR varies slowly with the temperature. Below 0°C the temperature dependency is stronger. Higher ESR is due to the increase of the electrolyte's viscosity at low temperatures limiting ionic transport speed which increases the resistance of the electrolyte.

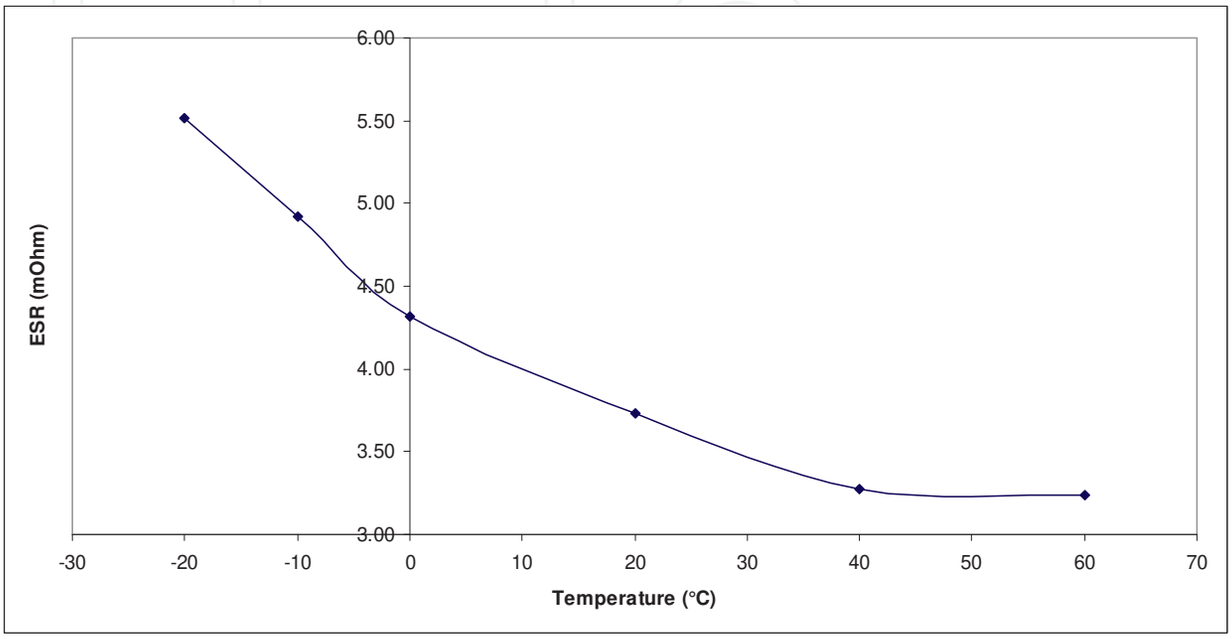

Figure 21. BCAP310F equivalent series resistance as function of temperature.

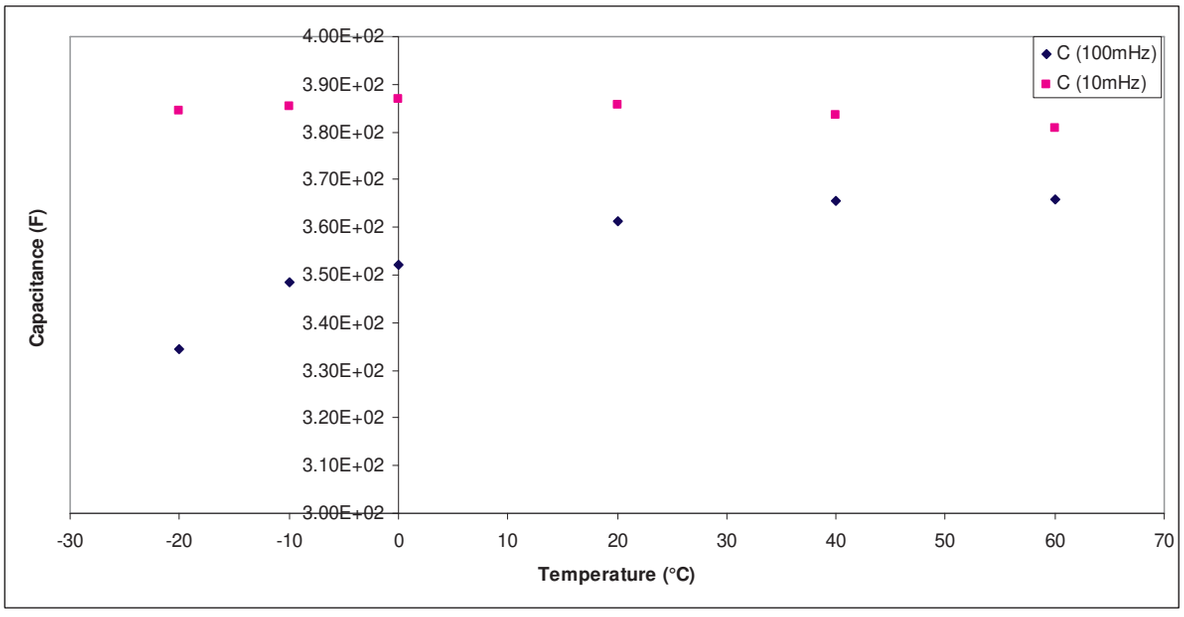

Figure 22. Capacitance evolution according to the temperature for 10mHz and 100mHz

http://dx.doi.org/10.5772/53490

In the case of the capacitance, the experimental results show that the capacitance is lower at negative temperature as shown in Figure 22. For example, at f=10mHz there is no variation of the capacitance with temperature. At 100mHz, C=335F at -20°C whereas C= 361F at 20°C. At negative temperature, the supercapacitor capacitance decreases with temperature.

In conclusion, it is clear that the supercapacitor electric performances and lifetime depend on the temperature.

3.3. Electrical modeling

In literature, several supercapacitors have been developed for different purposes [47-51]. In [47], a model has been proposed by Faranda et al (see Figure 23). The model exists of three branches. The first branch containing R0 represents the fast response of the supercapacitor in term of few seconds. The second branch contains a resistance and a large capacitor. Then the second branch demonstrates the long-term behavior in term of few minutes. However, the analysis that has been carried out by Chalmers University showed that the error between the simulated and experimental results for such model is in the range of 10%, which is statistically high.

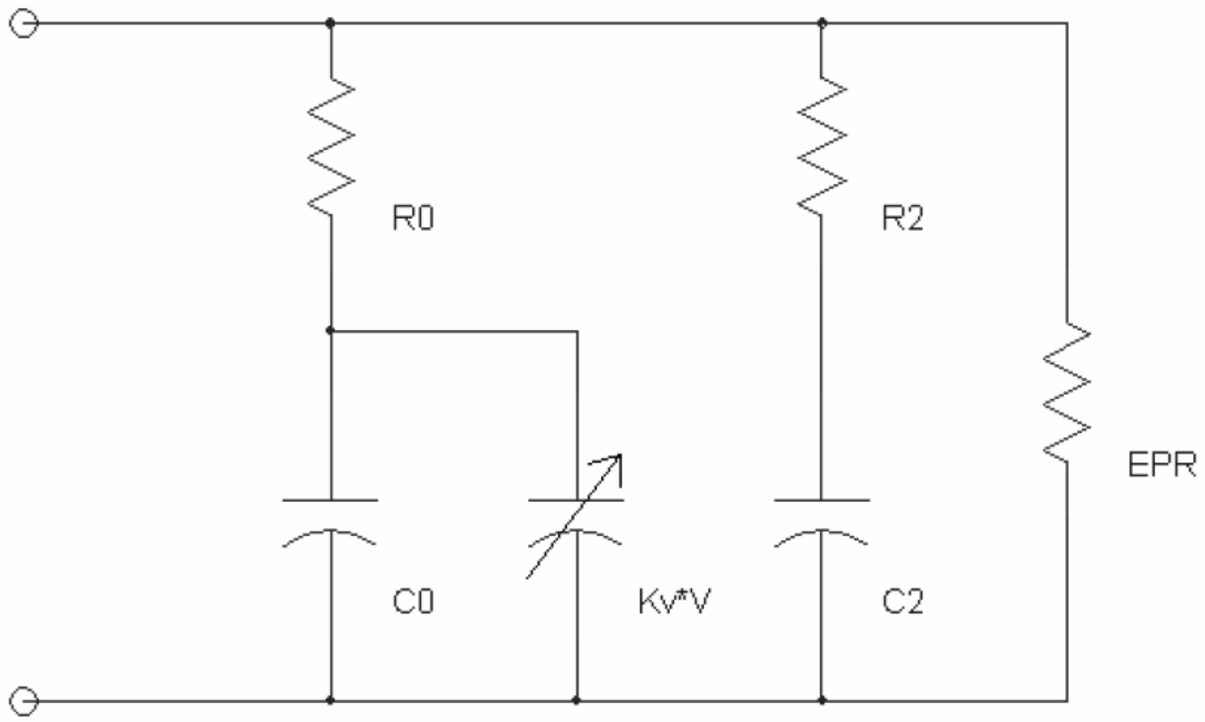

Figure 23. Three branches model [47]

In [48] a second order model has been proposed to demonstrate the supercapacitors behavior. The proposed model is strong similar to the second order Thévenin battery model. The model has significantly higher accuracy (error between the simulated and experimental results <5%) than the previous supercapacitor model due to the non-linear behavior of the model.

In [49-51] a new model has been developed based on electrochemical characterization of the supercapacitors on electrode and electrolyte level. Therefore, the model as presented in Figure 24 below has been proposed.

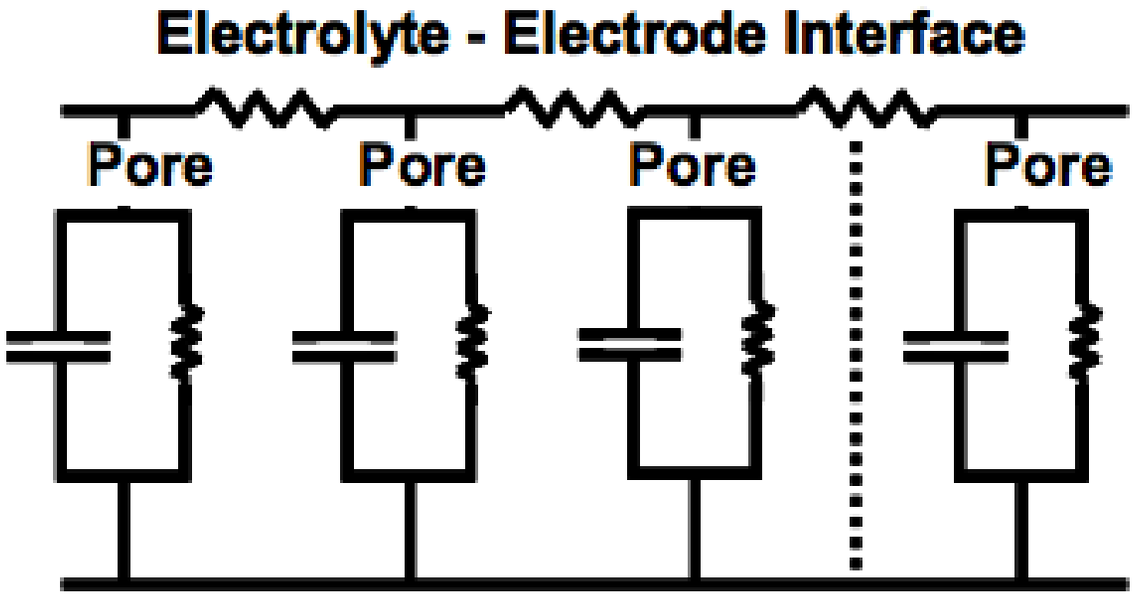

Figure 24. Electrochemical model [49-51]

Here it should be underlined that this model needs dedicated test procedures for determining the model parameters, which only can be carried out by chemists. Therefore, the use of the model in the vehicular applications is useless.

Then for the first two models, the model parameters can be extracted from the electrical approach. However, the simulation time and the complexity of such models is an obstacle in HEV applications. Therefore, in this section the model as presented in Figure 25 seems the most interesting model in real applications.

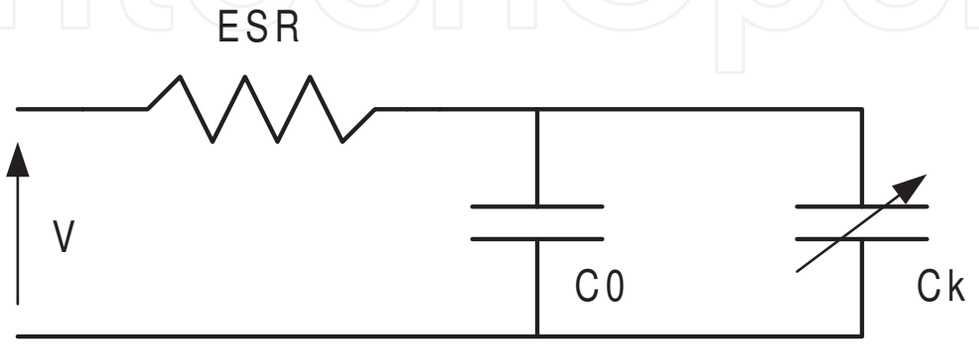

Figure 25. RCC model of the supercapacitor

http://dx.doi.org/10.5772/53490

A supercapacitor cell can be modeled by an equivalent RCC circuit as shown in Figure 25, where ESR is the series equivalent resistance, C0 is a constant capacitor and Ck=k*V varies according to the supercapacitor voltage. These parameters are identified by charging and discharging at constant current [40-46] and the obtained values for the BCAP310F were ESR=4.25mΩ, C0 = 282 F and Ck=46*V. This model is suitable for applications where the energy stored in the capacitor is of primary importance and the transient response can be neglected.

3.4. Thermal modeling

The thermal model developed is based on thermal-electric analogy and allows the determination of supercapacitor temperature inside and at the surface. The developed model can be easily implemented in different simulation programs. It can be used in the modeling of supercapacitors in order to study the heat management of a supercapacitors module. This model makes it possible to size the supercapacitors module cooling system when necessary. This is in order to maintain the temperature of the module within the operating temperature range given by the manufacturer. A Matlab/Simulink® simulation model was developed in order to calculate the R_{th} and C_{th} of a supercapacitor cell. Calculated values were compared to experimental values and the simulation model was validated. Thus a supercapacitor can be modeled as succession of RC and current source circuits. This application permits to calculate the evolution of the temperature in each layer of the supercapacitor cell. It can be used to perform detailed analysis of the temperature variation within a supercapacitor. When using supercapacitor modules which are composed of several cells in series and /or in parallel, it is necessary to study the thermal management of these modules [31]. The aim is to calculate and locate the maximum temperature in order to size the cooling system if needed. In this case, to reduce simulation time, the thermal model can be simplified as shown in Figure 26.

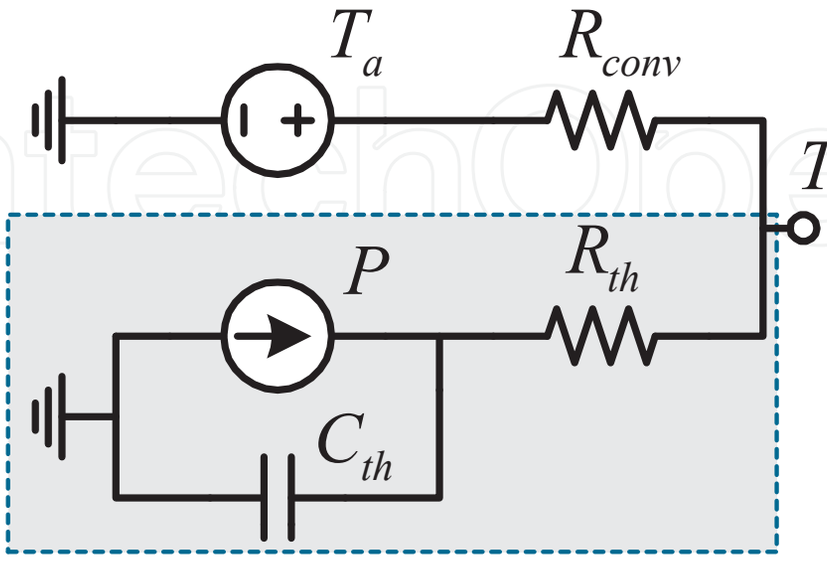

Figure 26. Thermal-electric model of the supercapacitor.

The thermal model gives the evaluation of the temperature on the external surface of the supercapacitor depending on the electrical power, the ambient temperature and the convective heat transfer coefficient. The total power dissipated in the supercapacitor is given by:

$$P(t) = ESR \times I^2(t) \tag{6}$$

Where:

- ESR : the equivalent series resistance of the supercapacitor,
- I(t) : the RMS current value passing through the supercapacitor.

The resistance R_{conv} represents the heat transfer between the surface of the supercapacitor and the ambient air. Its value depends on the convective heat transfer coefficient h and the heat exchange surface of the supercapacitor S_{sc}.

This coefficient can be calculated by using the following expression:

$$R_{conv} = \frac{1}{h \cdot S_{sc}} \tag{7}$$

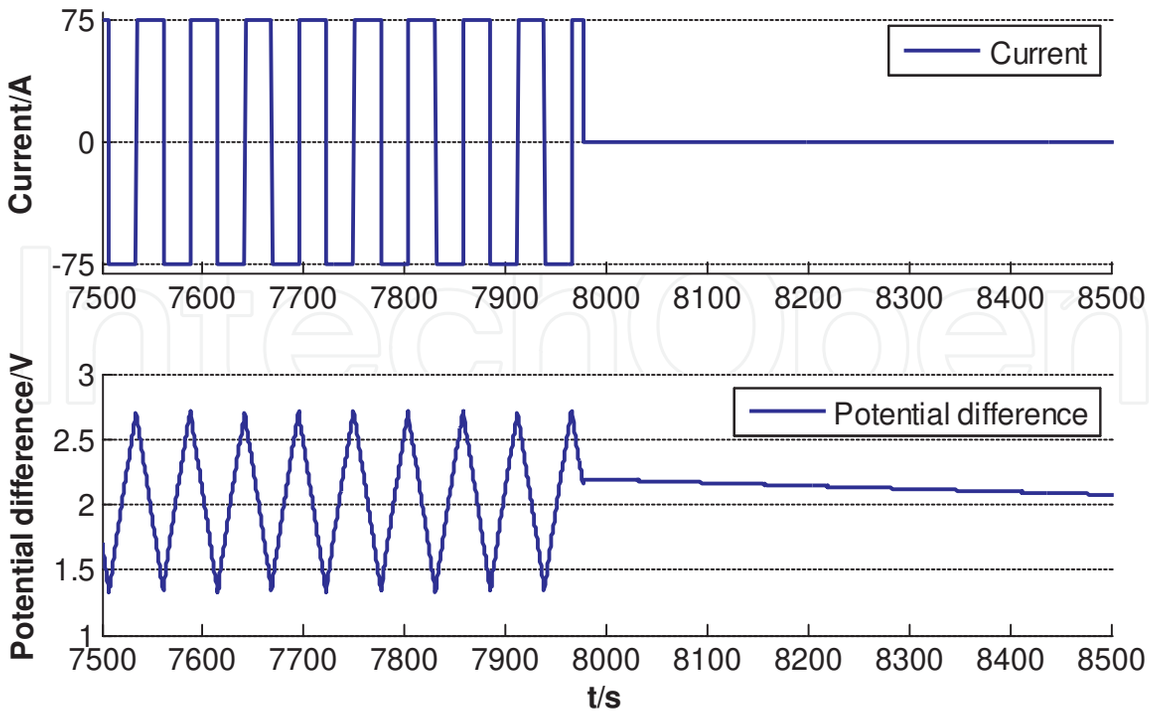

Figure 27. Current and voltage of the 1500F supercapacitor.

http://dx.doi.org/10.5772/53490

In order to validate this model, the parameters were calculated for a 1500F supercapacitor cell. This supercapacitor cell was experimentally tested; it was charged and discharged at 75A with a thermocouple type K placed on the outer surface. Figure 27 shows a zoom of the supercapacitor current and voltage during the receptive cycle which was applied to the 1500F supercapacitor. It shows the warming phase in which the supercapacitor is charged and discharged at 75A constant current then the phase of no cycling where the current is zero.

Figure 28 shows the evolution of the outside surface temperature of the 1500F supercapacitor. The warming phase is about 133 minutes where the supercapacitor is charged and discharged at 75A constant current. The ambient temperature is around 17.5°C.

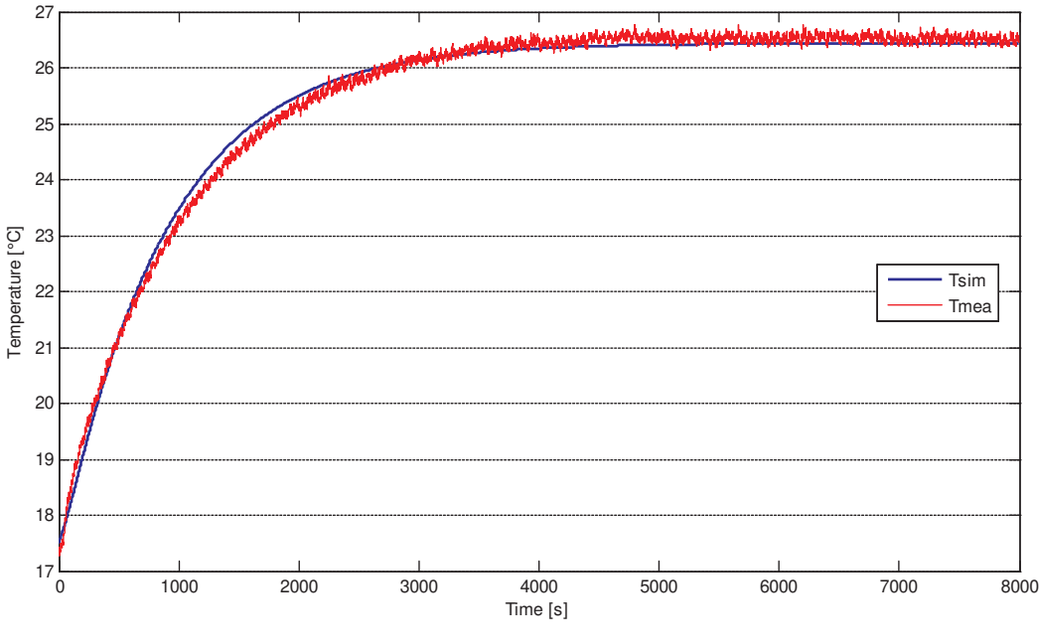

Figure 28. Evolution of measured and simulated temperatures of 1500F cell versus time (75A).

Results presented in Figure 28 show a good correlation between the experimental and simulation. Good agreements were also obtained with 10A and 20A constant currents for charging and discharging cycles.

4. Conclusion

In this chapter, the performance and characteristics of various lithium-ion based batteries are evaluated and discussed taking into account the power and energy densities, the capacity and the current rates. The evaluation is mainly based on the electrical and the thermal behavior. Different types of batteries were characterized at different current rates and different temperatures. The Peukert relationship was evaluated in function of various operating con-

ditions. Electrical and thermal models are developed and presented. The battery electrical model is based on the first order FreedomCar model. The parameters of the electrical model were obtained and calibrated based on a new developed test profile. A battery thermal model is proposed, discussed and validated. Electrical and thermal characterizations of supercapacitors were studied. The different basic calculation methods based on the EIS and the IEC 62576 of the Equivalent Series Resistance (ESR) and the capacitance of a supercapacitor are presented. An electrical model of the supercapacitor based on RCC circuit is presented. A thermal model of the supercapacitor is presented and it is based on the thermal-electric analogy. The model was validated using experimental results of the BCAP1500F supercapacitor cell. The simulation results of the thermal model can be used to find out if a cooling/heating system is necessary for the use of supercapacitor in order to improve its efficiency. The models developed are simple enough to be implemented in different simulation programs and thermal management systems for hybrid electric vehicles.

Author details

Monzer Al Sakka[1], Hamid Gualous[2], Noshin Omar[1] and Joeri Van Mierlo[1]

1 Vrije Universiteit Brussel, Belgium

2 Université de Caen Basse-Normandie, France

References

[1] G. Maggetto, J. Van Mierlo, Annales de Chimie – Science des matériaux, in: Thermatic Issue on "Material for Fuel Cell Systems", vol. 26, 2000, p. 9.

[2] J. Van Mierlo, G. Maggetto, Ph. Lataire, Energy Convers. Manage. 47 (2006) 196.

[3] P. Van den Bossche, F. Vergels, J. Van Mierlo, J. Matheys, W. Van Autenboer, J. Power Sources 26 (2005) 1277.

[4] N. Omar, F. Van Mulders, J. Van Mierlo, P. Van den Bossche, J. Asian Electric Vehicles 7 (2009) 1277.

[5] H. Abderrahmane, B. Emmanuel, Assessment of real behavior of VHE Energy Storage System in heavy vehicles, in: Proceeding of EET-2008 European Ele- Drive Conference, Geneva, March, 2008.

[6] N. Omar, B. Verbrugge, P. Van den Bossche, J. Van Mierlo, Electrochim. Acta 25 (2010) 7534.

[7] J. Cheng, J. VanMierlo, P. Van den Bossche, Ph. Lataire, Super capacitor based energy storage as peak power unit in the applications of hybrid electric vehicles, in: Proceeding of PEMD 2006, Ireland, 2006.

[8] C.R. Akli, X. Roboam, B. Sareni, A. Jeunesse, Energy management and sizing of a hybrid locomotive, in: Proceeding of EPE 2007, Denmark, 2007.

[9] Sh. Lu, K.A. Corzine, M. Ferdowsi, IEEE Trans. Veh. Technol. 56 (2007) 1516.

[10] N. Omar, M. Al Sakka, M. Daowd, Th. Coosemans, J. Van Mierlo, P. Van den Bossche, Assessment of behavior of active EDLC-battery system in heavy hybrid charge depleting vehicles, in: Proceeding of 4th European Symposium on Super Capacitors and Applications, Bordeaux, October, 2010.

[11] A. Cooper, M. Kellaway, Advanced lead-acid – the new battery system for hybrid electric vehicles, in: Proceeding of EET-2008 European Ele-Drive Conference, Geneva, March, 2008.

[12] N. Omar, M. Daowd, B. Verbrugge, G. Mulder, P. Van den Bossche, J. Van Mierlo, M. Dhaens, S. Pauwels, F. Leemans, Assessment of performance characteristics of lithium-ion batteries for PHEV vehicles applications based on a newly test methodology, in: Proceeding of the 25th World Battery, Hybrid and Fuel Cell Electric Vehicle Symposium, Shenzhen, November, 2010.

[13] N. Omar, B. Verbrugge, G. Mulder, P. Van den Bossche, J. Van Mierlo, M. Daowd, M. Dhaens, S. Pauwels, Evaluation of performance characteristics of various lithium-ion batteries for use in BEV application, in: Proceeding of IEEE Vehicle Power and Propulsion Conference, Lille, September, 2010.

[14] N. Omar, M. Daowd, G. Mulder, J.M. Timmermans, J. Van Mierlo, S. Pauwels, Assessment of performance of lithium ion phosphate oxide, nickel manganese cobalt oxide and nickel cobalt aluminum oxide based cells for using in plug-in battery electric vehicle applications, in: Proceeding of IEEE Vehicle Power and Propulsion Conference, Chicago, September, 2011.

[15] A. Burke, M. Miller, Performance characteristics of lithium-ion batteries of various chemistries for plug-in hybrid vehicles, in: Proceeding of the 24th World Battery, Hybrid and Fuel Cell Electric Vehicle Symposium, Stavanger, May, 2009.

[16] J. Axsen, Burke, K. Kurani, Batteries for Plug-in Hybrid Electric Vehicles (PHEVs): Goals and State of the Technology, May, 2008.

[17] N. Omar, M. Daowd, O. Hegazy, G. Mulder, J.M. Timmermans, Th. Coosemans, P. Van Den Bossche, J. Van Mierlo, Standardization work for BEV and HEV Applications: Critical Appraisal of Recent Traction Battery Documents. J. Energies 2012, 5, 138-156

[18] G. Mulder, N. Omar, S. Pauwels, F. Leemans, B. Verbrugge, W. De Nijs, P. Van den Bossche, D. Six, J. Van Mierlo, J, Enhanced test methods to characterise automotive battery cells. J. Power Sources 2011, 196, 100079 – 10087.

[19] IEC 61982-2, Secondary batteries for the propulsion of electric road vehicles - Part 2: Dynamic discharge performance test and dynamic endurance test, August 2002.

[20] A. Amine, C.H. Chen, J. Liu, J. Hammond, A. Jansen, D. Dees, I. Bloom, D. Vissers, G. Hendriksen, Factors responsible for impedance rise in high power lithium ion batteries, Vol. 97, No: 8, 2001, Jul., pp: 684-687.

[21] P. Van den Bossche, B. Verbrugge, N. Omar, J. Van Mierlo, The Electric Vehicle Charged by the Grid: Voltages and Power Levels, PHEV-09, September, 2009.

[22] IEC 61434, Secondary cells and batteries containing alkaline or other non-acid electrolytes - Guide to designation of current in alkaline secondary cell and battery standards, 1996.

[23] IEC 62660-1 Ed. 1: Secondary batteries for the propulsion of electric road vehicles – Part 1: Performance testing for lithium-ion cells, May, 2010.

[24] ISO 12405-1 Electrically propelled road vehicles – Test specification for lithium-ion traction battery packs and systems – Part 1: High- power applications. IEC, 2011.

[25] ISO 12405-2 Electrically propelled road vehicles – Test specification for lithium-ion traction battery packs and systems – Part 1: High- energy applications. IEC, 2011.

[26] K. Sawai, R. Yamato, T. Ohzuku, Impedance measurements on lithium-ion battery consisting of Li(Li1/3Ti5/3)O4 and LiCo1/2Ni1/2O2, Journal of Electrochemistry, No. 51, PP: 1651-1655.

[27] M. Daowd, N. Omar, P. Van den Bossche, J. Van Mierlo, A Review of Passive and Active Battery Balancing based on MATLAB/Simulink, INTERNATIONAL REVIEW OF ELECTRICAL ENGINEERING-IREE, Vol. 6, pp: 2974–2989, 2011

[28] M. Daowd, N. Omar, P. Van den Bossche, J. Van Mierlo, Extended PNGV Battery Model for Electric and Hybrid Vehicles, INTERNATIONAL REVIEW OF ELECTRICAL ENGINEERINGIREE, Vol. 6, pp: 1264–1278, 2010

[29] V.H. Johnson, A. Pesaran, Th. Sack, Temperature-dependent battery models for high-power lithium-ion batteries. Proceedings EVS-17, October 2000, Montréal, Canada.

[30] N. Omar, M. Al Sakka, M. Daowd, O. Hegazy, Th. Coosemans, P. Van den Bossche, J. Van Mierlo, Development of a Thermal Model for Lithium–Ion Batteries for Plug-In Hybrid Electric Vehicles, Proceedings EVS 26, 2012, Los Angeles, USA

[31] M. Al Sakka, Gualous H., Van Mierlo J., and Culcu H. Thermal modeling and heat management of supercapacitor modules for vehicle applications. Journal of Power Sources, 194:581–587, 2009.

[32] Monzer Al Sakka: Supercapacitors and DC/DC Converters for Fuel Cell Electric Vehicle, PhD at Vrije Universiteit Bruseel, Brussels, September 2010, ISBN: 978 90 5487 802 5.

[33] IEC 62576, Electric Double-Layer Capacitors for Use in Hybrid Electric Vehicles - Test Methods for Electrical Characteristics, IEC, 2008.

[34] Yonghua Cheng, "Assessement of Energy Capacity and Energy Losses of supercapacitors in Fast Charging-Discgarging Cycles", Energy Conversion, IEEE Transactions, Volume : 25, Issue. 1, pp. 253 – 261, 2010.

[35] R. Kötz, M. Hahn, R. Gallay, "Temperature behaviour and impedance fundamentals of supercapacitors", Journal of Power Sources, 154 (2006) pp. 550–555, 2006.

[36] H. Gualous, D. Bouquain, A. Berthon, J. M. Kauffmann "Experimental study of supercapacitor serial resistance and capacitance variations with temperature" Journal of Power Sources, Vol. 123, pp.86-93, 2003.

[37] F. Rafik, H. Gualous, R. Gallay, A. Crausaz, A. Berthon "Frequency, thermal and voltage supercapacitor characterization and modelling", Journal of Power Sources, Vol. 165, pp. 928-934, 2007.

[38] Oliver Bohlen, Julia Kowal, Dirk Uwe Sauer "Ageing behaviour of electrochemical double layer capacitors: Part II. Lifetime simulation model for dynamic applications" Journal of Power Sources, Volume 173, Issue 1, Pages 626-632, 2007.

[39] Y. Diab; P. Venet, H. Gualous, G. Rojat, "Self-Discharge Characterization and Modeling of Electrochemical Capacitor Used for Power Electronics Applications" IEEE Transactions On Power Electronics. Vol. 24, Issue 2, pp. 510-517, 2009.

[40] F. Rafik, H. Gualous, R. Gallay, A. Crausaz, A. Berthon, "Supercapacitors characterization for hybrid vehicle applications", Proc. IEEE 5th Power Electronics and Motion Control Conference, Shanghai, China, pp. 1-5, 2006.

[41] A. Hammar, R. Lallemand, P. Venet, G. Coquery, G. Rojat, J. Chabas, "Electrical characterization and modelling of round spiral supercapacitors for high power applications", Proc. 2nd European Symp. on Super Capacitors & Applications, Lausanne, Switzerland, 2006.

[42] L. Zubieta, R. Bonert, "Characterization of double-layer capacitors for power electronics applications", Proc. IEEE 33rd Industrial Applications Society annual meeting, St. Louis, MO, USA, pp. 1149 – 1154, 1998

[43] L. Zubieta, R. Bonert, "Characterization of double-layer capacitors for power electronics applications", IEEE Transactions on Industry Applications Vol. 36 Issue 1, pp. 199-205, 2000.

[44] John M. Miller, Uday Deshpande, Marius Rosu, "CarbonCarbon Ultracapacitor Equivalent Circuit Model, Parameter Extraction, and Application", Maxwell Technologies, Inc Ansoft Corp. San Diego, CA Pittsburg, PA, Ansoft First Pass Workshop, Southfield, 2007.

[45] Bavo Verbrugge, Frederik Van Mulders, Hasan Culcu, Peter Van Den Bossche, Joeri Van Mierlo, "Modelling the RESS: Describing Electrical Parameters of Batteries and Electric Double-Layer Capacitors through Measurements", World Electric Vehicle Journal, Vol. 3, 2009.

[46] Joeri Van Mierlo, Gaston Maggetto, Peter Van Den Bossche Impact, “Models of Energy Sources for EV and HEV: Fuel cells, Batteries, Ultra-Capacitors, Flywheels and Engine-generators”, Journal of Power Sources, Vol. 28, N° 128, pp: 76 - 89, 2004.

[47] Faranda, R.; Gallina, M.; Son, D.T.; A new simplified model of Double-Layer Capacitors 2007; ICCEP '07. International Conference on Clean Electrical Power 21-23 May 2007 Page(s):706 – 710; ISBN: 1- 4244-0632-3

[48] Data sheet for supercapacitor from EPCOS with Part No.: B48621-S0203-Q288

[49] Qu, D. Y. and H. Shi (1998). "Studies of activated carbons used in double-layer capacitors." Journal of Power Sources 74(1): 99-107.

[50] Shi, H. (1996). "Activated carbons and double layer capacitance." Electrochimica Acta 41(10): 1633-1639.

[51] Vix-Guterl, C., E. Frackowiak, et al. (2005). "Electrochemical energy storage in ordered porous carbon materials." Carbon 43(6): 1293-1302.